Promotion effect of rare earth elements (Ce, Nd, Pr) on physicochemical properties of M-Al mixed oxides (M = Cu, Ni, Co) and their catalytic

(article starts on next page)

Chemical routes to materials

Promotion effect of rare earth elements (Ce, Nd, Pr) on physicochemical properties of M-Al mixed oxides (M = Cu, Ni, Co) and their catalytic activity in N₂O decomposition

Phuoc Hoang Ho[1,2,3,7], Magdalena Jabłońska[1,4,5,*] , Giada Beltrami[6], Annalisa Martucci[6], Thomas Cacciaguerra[3], Werner Paulus[3], Francesco Di Renzo[3,*], Giuseppe Fornasari[2], Angelo Vaccari[2], Patricia Benito[2,*], and Regina Palkovits[1,4]

[1] *Chair of Heterogeneous Catalysis and Chemical Technology, RWTH Aachen University, Worringerweg 2, 52074 Aachen, Germany*
[2] *Department of Industrial Chemistry "Toso Montanari", Alma Mater Studiorum, Università Di Bologna, Viale Risorgimento 4, 40136 Bologna, Italy*
[3] *ICGM, Univ Montpellier-CNRS-ENSCM, 240 Avenue Emile Jeanbrau, 34296 Montpellier, France*
[4] *Center for Automotive Catalytic Systems Aachen, RWTH Aachen University, Schinkelstr. 8, 52062 Aachen, Germany*
[5] *Institute of Chemical Technology, Universität Leipzig, Linnéstr. 3, 04103 Leipzig, Germany*
[6] *Department of Physics and Earth Science, University of Ferrara, Via Saragat 1, 44122 Ferrara, Italy*
[7] *Present address: Chemical Engineering, Competence Centre for Catalysis, Chalmers University of Technology, 412 96 Gothenburg, Sweden*

ABSTRACT

A series of M-AlO$_x$ mixed oxides (M = Cu, Co, Ni) with the addition of high loadings of rare earth elements (REE, R = Ce, Nd, Pr; R$_{0.5}$M$_{0.8}$Al$_{0.2}$, molar ratio) were investigated in N₂O decomposition. The precursors were prepared by coprecipitation and subsequent calcination at 600 °C. The obtained mixed metal oxides were characterized by X-ray diffraction with Rietveld analysis, N₂ sorption, and H₂ temperature-programmed reduction. Depending on the nature of REE and the initial M-Al system, R cations could be separately segregated in oxide form or coordinated with the transition metal cations and form mixed structures. The addition of Ce^{3+} consistently led to nanocrystalline CeO₂ mixed with the divalent oxides, whereas the addition of Nd^{3+} or Pr^{3+} resulted in the formation of their respective oxide phases as well as perovskites/Ruddlesden–Popper phases. The presence of REE modified the textural and redox properties of the calcined materials. The rare earth element-induced formation of low-temperature reducible MO$_x$ species that systematically improved the N₂O decomposition on the modified catalysts compared to the pristine M-Al

Address correspondence to E-mail: magdalena.jablonska@uni-leipzig.de; Francesco.Di-Renzo@enscm.fr; patricia.benito3@unibo.it

materials by the order of Co > Ni > Cu. The $Ce_{0.5}Co_{0.8}Al_{0.2}$ catalyst revealed the highest activity and remained stable (approximately 90% of N_2O conversion) for 50 h during time-on-stream in 1000 ppm N_2O, 200 ppm NO, 20 000 ppm O_2, 2500 ppm H_2O/N_2 balance at WHSV = 16 L g^{-1} h^{-1}.

Introduction

Nitrous oxide (N_2O), an inevitable by-product from adipic and nitric acid production plants, is a recognized global warming agent and contributes to the degradation of the stratospheric ozone layer. N_2O, with a global warming potential factor 265–298 times higher than that of CO_2, persists in the atmosphere for as long as 150 years [1, 2]. The catalytic decomposition of N_2O (deN_2O) is one of the most appropriate solutions to abate nitrous oxide from large emissions of industrial sources. The process presents the distinct advantage of not requiring the addition of any specific reagent, as required in the selective catalytic oxidation or N_2O reduction [3]. In this regard, the development of a highly efficient and stable catalyst derived from cheap elements is required for industrial application. Over the past decades, the use of a variety of materials as catalysts for deN_2O has been reviewed and classified by either the active phase (e.g., noble or transition metals) or the support (e.g., zeolites, metal oxides, hexaaluminate, perovskites, spinels, hydrotalcite-derived mixed metal oxides, etc.) [2–6]. Among them, transition metal-based materials, especially Cu, Ni, and Co mixed oxides derived from hydrotalcite-like (HT) compounds, were reported as highly efficient catalysts. In an early study, Kannan reported that CuAl, NiAl, and CoAl mixed oxides derived from respective HT showed activity in deN_2O by using 0.1 g of catalyst, 0.0985 vol. % N_2O/He, a total flow rate of 100 cm^3 min^{-1}, 450 °C [7]. NiAl-O_x and CoAl-O_x revealed N_2O conversion of 84–95% compared to the conversion of 48% for CuAl-O_x. The activity was improved when increasing the molar ratio M/Al from 1.0 up to 3.0, where the highest activity in deN_2O was achieved.

Among rare-earth-doped materials, high activity in deN_2O was given for Rh-supported materials (e.g., $Rh/Ce_{1-x}Pr_xO_2$) [8–10] or perovskite-based materials (e.g., $Pr_{1-x}Ba_xMnO_3$, $LnSrLeO_4$) [11–15]. Several studies focused on the development of mixed oxide

catalysts containing an active phase of transition metals (Cu, Ni, Co) modified by REE, mainly with Ce [16–27]. Albeit these catalysts are promising, allowing high conversion of N_2O even in presence of O_2 [20, 26], they are still sensitive to H_2O [18, 25]. Their catalytic activity can also be improved significantly with an introduction of alkali or alkali earth metals as promoters [28, 29]. Besides Ce, some recent works have proposed Nd as a promising promoter [30, 31]. In a previous study, Ho et al. reported that the addition of an optimum loading of Nd improved significantly the activity of modified CuAl-O_x and CoAl-O_x [32]. Although Nd is classified into the rare-earth group, its abundance reaches 38 mg kg^{-1}, which is the second highest in the group [33]. The two left-neighbor of Nd, Ce and Pr, are also not particularly rare, making up 60 and 9.1 mg kg^{-1} of Earth's crust [33]. Although Ce, Pr, and Nd are three sequential elements in the periodic table, a different configuration of outer electron arrangement results in a differently stable oxidation state in oxides, e.g., + 4 for Ce, a mixture of + 4/ + 3 for Pr, and + 3 for Nd. Such difference in stable oxidation state is expected to create different interactions with the active phase, e.g., Cu, Ni, or Co in form of mixed oxides. Ho et al. showed that Nd^{3+} interacts with Cu^{2+}/Al^{3+} or Co^{2+}/Al^{3+} during coprecipitation resulting in the formation of $CuNd_2O_4$ Ruddlesden–Popper phase for the former but $NdCoO_3$ perovskite in the latter case, and in both cases, the catalytic activity in deN_2O was significantly improved [32].

REE (e.g., Y^{3+}, Dy^{3+}, Gd^{3+}, Sm^{3+}, La^{3+}) can be possibly incorporated into Mg–Al HT during coprecipitation with low loading, e.g., 2% mole of total cations [34]. However, the incorporation of REE into the brucite layer of the HT structure is challenging due to the large size of their cations. As a consequence, increasing the fraction of rare earth cations leads to the segregation of their carbonate or hydroxycarbonate phases apart from HT [35]. Those materials after calcination are expected to have distinct properties due to the different interactions of rare earth cations with other elements in the

precursor phases. Zhang et al. found that the high content of La^{3+} in Ni/γ-Al_2O_3 could enhance the dispersion of NiO by the formation of NiO microcrystallites separated by La_2O_3 [36]. Moreover, they also stated that there are interactions between La_2O_3 and Al_2O_3 or, to a lesser extent, NiO and Al_2O_3, to form $LaAlO_3$ or $NiAl_2O_4$, respectively. Ho et al. showed that, in the catalysts obtained by the addition of Nd^{3+} in Cu/Al or Co/Al nitrate precursors, Nd^{3+} presented a complex behavior. It not only interacted with divalent cations and Al^{3+} but also simultaneously formed isolated phases of Nd such as oxide or oxycarbonate [32]. Such interactions created both active and less active phases for catalytic deN_2O depending on the amount of Nd^{3+} addition. To the best of our knowledge, there are only a few reports regarding the application of mixed metal oxides containing REE introduced during the coprecipitation step. The present study aims at providing a broad picture of the effects of different REE (R = Nd, Pr, Ce) on the physicochemical properties of R/M/Al mixed oxides (M = Cu, Co, Ni). A series of catalysts were prepared by coprecipitation of mixed nitrate precursors of R^{3+}, M^{2+}, and Al^{3+} ($R^{3+}/M^{2+}/Al^{3+}$ = 0.5/0.8/0.2 molar ratio) followed by a calcination step, characterization, and testing for N_2O decomposition. A thorough evaluation of XRD data was performed to understand the main interactions of each REE with M and Al, and quantify the phase fraction of different polyphasic samples. This information connected with the redox properties of the materials, allowed us to propose correlations with the catalytic activity in N_2O decomposition.

Experimental part

Catalyst preparation

A series of $M_{0.8}Al_{0.2}$ and $R_{0.5}M_{0.8}Al_{0.2}$ (where R = Ce, Nd, Pr; M = Cu, Ni, Co) mixed metal oxides were prepared by coprecipitation followed by thermal treatment in air. These molar ratios were selected based on the screening tests reported by Ho et al. [32]. In a typical experiment, 1 M aqueous solution of the metal precursors ($Nd(NO_3)_3 \cdot 6H_2O$ (99.9%, Sigma), $Pr(NO_3)_3 \cdot 6H_2O$ (99.9%, Sigma), $Ce(NO_3)_3 \cdot 6H_2O$ (99.99%, Sigma), $Ni(NO_3)_2 \cdot 6H_2O$ (98.5%, Sigma), $Co(NO_3)_2 \cdot 6H_2O$ (98%, Sigma), $Cu(NO_3)_2 \cdot 3H_2O$ (99%, Sigma), and $Al(NO_3)_3 \cdot 9H_2O$ (98%, Sigma) with given

molar composition was added dropwise to a solution of Na_2CO_3 (anhydrous 99.5%, Sigma) under vigorous stirring at 60 °C. The amount of carbonate anion used was 1.5-fold the stoichiometric ratio required for the charge balance of hydrotalcite-like compounds. The pH was constantly controlled at 10 ± 0.1 by using 1.0 M NaOH (98.8%, Chemsolute) solution. The resulted slurry was aged for 0.5 h at 60 °C before being filtered and washed thoroughly with warm distilled water until neutral pH. The final product was dried at room temperature for 24 h and subsequently calcined at 600 °C for 6 h in static air. The catalysts were denoted as MAl or RMAl corresponding to the composition of the cation solution used for preparation. Mixed oxide catalysts were stored in a desiccator to avoid the reconstruction of the precursor structure. For comparison purposes, pure transition metal oxides (CuO, NiO, and Co_3O_4) were also prepared with the same protocol using respective nitrate solutions without REE. For catalytic tests, the materials were crushed and the fraction in the range of 0.25–0.50 mm particle size was collected to use.

Catalysts characterization

X-ray diffraction (XRD) measurements of the calcined powders were performed using a Bruker D8 Bragg–Brentano Theta–Theta diffractometer with Cu-Kα radiation (λ = 1.54056 Å, 40 kV, 40 mA) in 2θ range of 5–80° with a step size of 0.02° and scan step time of 10.6 s. The EXPGUI v.1251 interface [37] for the GSAS program [38] was used for Rietveld refinements. The diffraction peak profile was modeled by a pseudoVoigt function, which included Gaussian and Lorentzian broadening coefficients, plus an asymmetry contribution. Besides that, a shifted Chebyshev polynomial was employed to reproduce the background. The Rietveld method was also used to determine the accurate model phase fractions of different polyphasic samples obtained in the optimized procedure. The standard deviation is 1%.

N_2 adsorption/desorption measurements were performed at -196 °C using a Micromeritics ASAP 2020 instrument. Catalysts (~ 0.15 g) were outgassed under vacuum (<30 mTorr) at 250 °C for 6 h before doing the measurement. The specific surface area (S_{BET}) was calculated by linearization of the Brunauer–Emmett–Teller (BET) relation in the relative pressure range around the monolayer volume.

Mesopore size distribution was evaluated by a DFT kernel and the total pore volume V_p was calculated at $p/p_0 = 0.975$, corresponding to an ideal cylindrical pore diameter of 50 nm [39].

The H_2 temperature-programmed reduction (H_2-TPR) of mixed metal oxides was performed using an AutoChem II Chemisorption analyzer (Micromeritics). Prior to measurement, catalysts (50 mg) were activated at 600 °C for 1 h in pure Ar (20 mL min^{-1}), and subsequently cooled down to 40 °C. H_2-TPR runs were carried out from 40 to 950 °C, with a ramping rate of 10 K min^{-1} and in a flow (30 mL min^{-1}) of 3 vol.% H_2/Ar.

Catalytic tests

The experiments were carried out under atmospheric pressure in a fixed-bed flow microreactor (i.d., 8 mm; l., 320 mm). Prior to the reaction, the catalysts (300 mg, particle size 0.25–0.50 mm) were outgassed at 600 °C for 0.5 h in a flow of pure N_2 (80 mL min^{-1}). The catalysts were then cooled down to 50 °C under the same N_2 flow before switching to the reactant flow. The total flow rate of the feed stream was 80 mL min^{-1}, controlled by mass flow controllers. The reactant composition at the reactor inlet was 1000 ppm N_2O in N_2 as balance. The most active catalyst was further studied in harsh reaction conditions by adding inhibitors: 200 ppm NO, 20 000 ppm O_2, 2500 ppm H_2O (applying temperature-controlled saturator). Outlet stream was analyzed by infrared spectroscopy using an Agilent Cary 660 equipped with a Pike 2 m heated gas cell. The temperature was raised in steps of 50 °C starting from 50 up to 600 °C. Each temperature was set constant for 0.5 h. The stability test was carried out at a constant temperature of 450 °C for 50 h with the presence of the inhibitors. The conversion of N_2O ($X(N_2O)$) was estimated according to $X(N_2O) = ([c(N_2O)_{in} - c(N_2O)_{out}]/c(N_2O)_{in}) \times 100$, where: $c(N_2O)_{in}$ and $c(N_2O)_{out}$ are, respectively, the concentration of N_2O in the inlet gas and the concentration of N_2O in the outlet gas.

The apparent activation energy (E_a) was calculated from the slope of linear regression derived from Arrhenius equation $k = A \cdot e^{-(E_a/RT)}$, where k was calculated from a kinetic model for the flow reactor with the assumption of the first-order reaction $k\tau = X_{N_2O}/(1 - X_{N_2O})$. In which k (s^{-1}) is reaction rate, A is the pre-exponential factor, E_a (kJ mol^{-1}) is the apparent activation energy, R (J mol^{-1} K^{-1}) is ideal gas law constant, T (K) is temperature, τ (s) is space–time and X_{N_2O} (%) is N_2O conversion. Detailed information can be found elsewhere [32].

Results and discussion

Phase composition of the catalysts

The XRD patterns of the precipitated precursors in the absence of REE presented nanocrystalline LDH (layered double hydroxides, hydrotalcite-like) patterns. For synthesis in the presence of REE, only amorphous precipitates were formed. This indicates that the rare earth cations were in close interaction with divalent and Al cations, preventing the formation of LDH phases (by decreasing the ratio of divalent/plurivalent cations below the threshold of formation of LDH).

Figure 1 presents the XRD patterns of mixed metal oxides after calcination at 600 °C. A quantitative evaluation of the crystalline phases present, as obtained by Rietveld refinement, is reported in Table 1. This evaluation of the amount of phases is unable to take into account non-crystalline amorphous materials. Further, details on the phases can be found in supplementary materials Table S1.

The XRD patterns of samples (calcined at 600 °C) prepared in the absence of REE present one crystalline phase: CuO tenorite, NiO bunsenite, or Co_3O_4 cobalt spinel, respectively, for CuAl, NiAl, or CoAl samples. No phases explicitly containing aluminum are observed for these samples, which are expected to contain a large amount of Al-rich amorphous material. Indeed, Al-containing spinel phases are observed only for calcination temperatures of 750–850 °C for Ni–Al or Ni,Cu-Al HT [40, 41]. However, due to the very limited swelling of the spinel cell parameter with the replacement of Co^{3+} by Al^{3+} in the octahedral site of Co_3O_4, it is impossible to infer from the cell size if some Al is incorporated in the cobalt spinel [42].

All REE-bearing samples presented the oxide phases of the transition elements, accompanied by different rare-earth or mixed transition element-rare earth oxides. Cerium was always present as CeO_2 cerianite and never formed mixed phases. Neodymium mixed phases were formed as Ruddlesden–Popper phases, namely Nd_2CuO_4 as the main phase
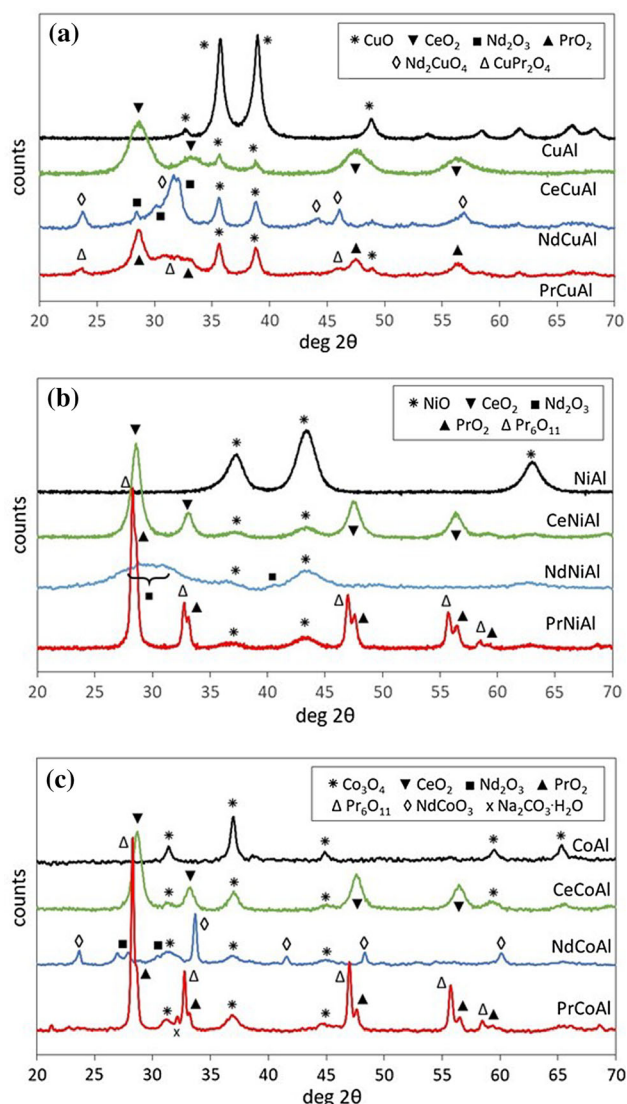
Figure 1 XRD patterns of (A) Cu-, (B) Ni-, (C) Co-containing catalysts.

in NdCuAl and NdCoO$_3$ perovskite in NdCoAl. The addition of praseodymium lead to the formation of Ruddlesden–Popper phase—CuPr$_2$O$_4$ in PrCuAl; however, no mixed phases with cobalt appeared. The mixed phases were always accompanied by varying amounts of rare earth oxides. PrO$_2$ was present in all Pr-bearing samples but it was accompanied by significant amounts of partially reduced Pr$_6$O$_{11}$ in PrNiAl and PrCoAl. Nd$_2$O$_3$ formed different phases in the presence of different transition metal cations: a minor amount of hexagonal P63/mmc in NdCuAl, monoclinic C2/m in NdNiAl, and cubic Ia-3 in NdCoAl, accompanied by a minor amount of hexagonal P63/mmc. The stabilization of cubic

Sc$_2$O$_3$-type phase (as a representative structure for all oxides from lanthanide group) was reported in the case of nucleation inside an amorphous aluminate matrix [43], whereas the presence of divalent cations promoted the formation of monoclinic Nd$_2$O$_3$ [44].

Textural properties of the catalysts

The values of specific surface area, pore volume, and mesopore size of the materials calcined at 600 °C are reported in Table 1. Despite the presence of significant amounts of amorphous alumina in all samples, the specific surface area is reasonably correlated to the crystallite sizes evaluated by the Scherrer method, reported in Table S1. For the materials without REE, the specific surface area, respectively, 65, 133, and 59 m^2 g^{-1} for CuO, NiO and Co$_3$O$_4$, exhibited an inverse relationship with the crystallite size of 11, 4, and 15 nm, respectively. In the presence of rare earth cations, the crystallite size of CuO and NiO was virtually unchanged, whereas the crystallite size of Co$_3$O$_4$ was nearly halved, as shown in Fig. 2A.

The evolution of the specific surface area with the incorporation of REE was in most cases accountable by the formation of new phases with a different crystallite size. The only instance of increase of specific surface area with the introduction of REE was observed for CeCuAl, due to the presence of CeO$_2$ nanocrystals of 4 nm, much smaller than the CuO crystallite present. The crystallite size of CeO$_2$ was nearly double in other preparations, for which the presence of the REE corresponded to a decrease of specific surface area. A similar specificity of the presence of copper species was observed in the case of PrO$_2$, for which the crystallite size increased from 6 nm in PrCuAl to 15–20 nm in PrNiAl and PrCoAl. Pr$_6$O$_{11}$ presented slightly larger crystallite size. The Ruddlesden–Popper and perovskite phases presented crystallite sizes in the range of 12–15 nm Nd$_2$O$_3$ phases present very small crystallites and the evaluation of their size is quite unreliable.

The specific surface area values are also affected by the level of aggregation of particles, on which the evaluation of the porosity of the materials provides some information. N$_2$ sorption isotherms and mesopore size distributions are shown in Fig. 3, whereas the values of mesopore volume and the position of the highest peak of the pore size distribution are reported in Table 1. The oxides formed in the absence of REE present quite different distributions of

**Table 1** Phase composition and textural properties of catalysts

Sample code	Crystalline phases [a]	Specific surface area / m^2 g^{-1}	Pore volume / cm^3 g^{-1}	Mesopore size / nm[d]
CuAl	CuO (100)	65	0.23	36
CeCuAl	CuO (39), CeO$_2$ (61)	76	0.43	8
NdCuAl	CuO (46), Nd$_2$O$_3$[b] (6), Nd$_2$CuO$_4$ (48)	35	0.28	21
PrCuAl	CuO (41), PrO$_2$ (32), CuPr$_2$O$_4$ (27)	17	0.40	37
NiAl	NiO (100)	133	0.11	6
CeNiAl	NiO (51), CeO$_2$ (49)	85	0.13	15
NdNiAl	NiO (53), Nd$_2$O$_3$[b] (47)	41	0.13	60
PrNiAl	NiO (43), PrO$_2$ (37), Pr$_6$O$_{11}$ (20)	47	0.14	13
CoAl	Co$_3$O$_4$ (100)	59	0.10	10
CeCoAl	Co$_3$O$_4$ (41), CeO$_2$ (59)	51	0.14	47
NdCoAl	Co$_3$O$_4$ (40), Nd$_2$O$_3$[b] (28), NdCoO$_3$ (32)	33	0.11	8
PrCoAl	Co$_3$O$_4$ (43), PrO$_2$ (26), Pr$_6$O$_{11}$ (31)[c]	30	0.12	8

[a]In parenthesis: mass percent on crystalline phases by Rietveld refinement

[b]Nd$_2$O$_3$ phases: hexagonal P63/mmc in NdCuAl, monoclinic C2/m in NdNiAl, 4% hexagonal P63/mmc and 24% cubic Ia-3 in NdCoAl

[c]Traces of Na$_2$CO$_3$·H$_2$O were observed

[d]Mode of the distribution
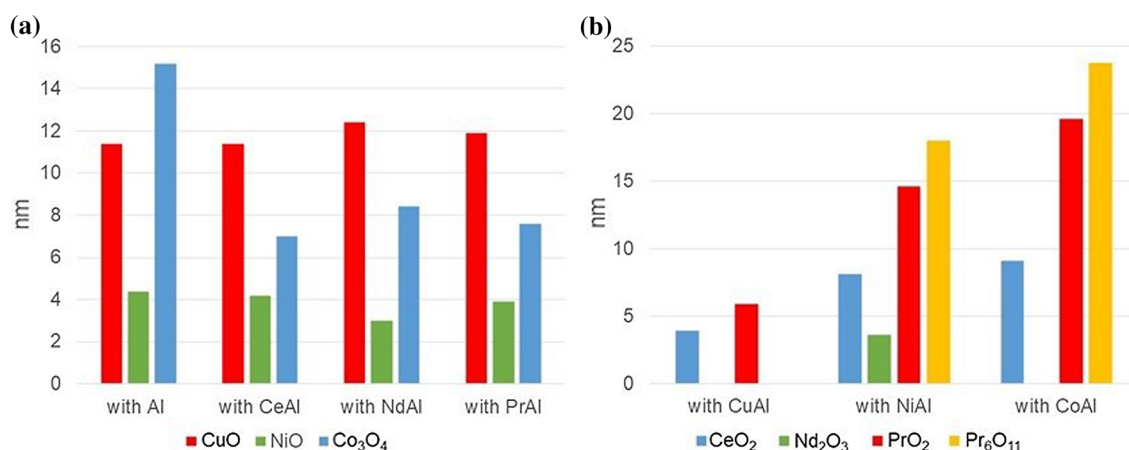
Figure 2 Evolution of the Scherrer crystallite size of (A) transition metal oxides in the presence of different REE and (B) rare earth oxides in the presence of different transition metals.

porosity. CuAl possessed a very broad distribution of large mesopores, with a shallow maximum near 40 nm. It is interesting to compare this value with the Gurvitch value. The Gurvitch relationship D = 4 V/ S, where V is the pore volume and S is the specific surface area per unit mass, allows calculating the so-called hydrodynamic diameter, which provides a rough evaluation of the pore size of uniform pore distribution [45, 46]. The measured pore volume of the CuAl sample is more than twice the value calculated by the Gurvitch correlation from values of specific surface area and pore diameter. This effect, related to the broadness of the pore size distribution, corresponds to a loose of hierarchical organization of aggregates of nanoparticles, which increases the accessibility of the intergranular porosity. This kind of organization is shared by the Cu-bearing rare earth materials, which presented a similarly broad distribution of pore size and a pore volume higher than the Gurvitch estimate. The pore volume of CuAl increased in the presence of high-specific surface area CeO$_2$ nanoparticles and decreased in the presence of Nd and Pr mixed phases.
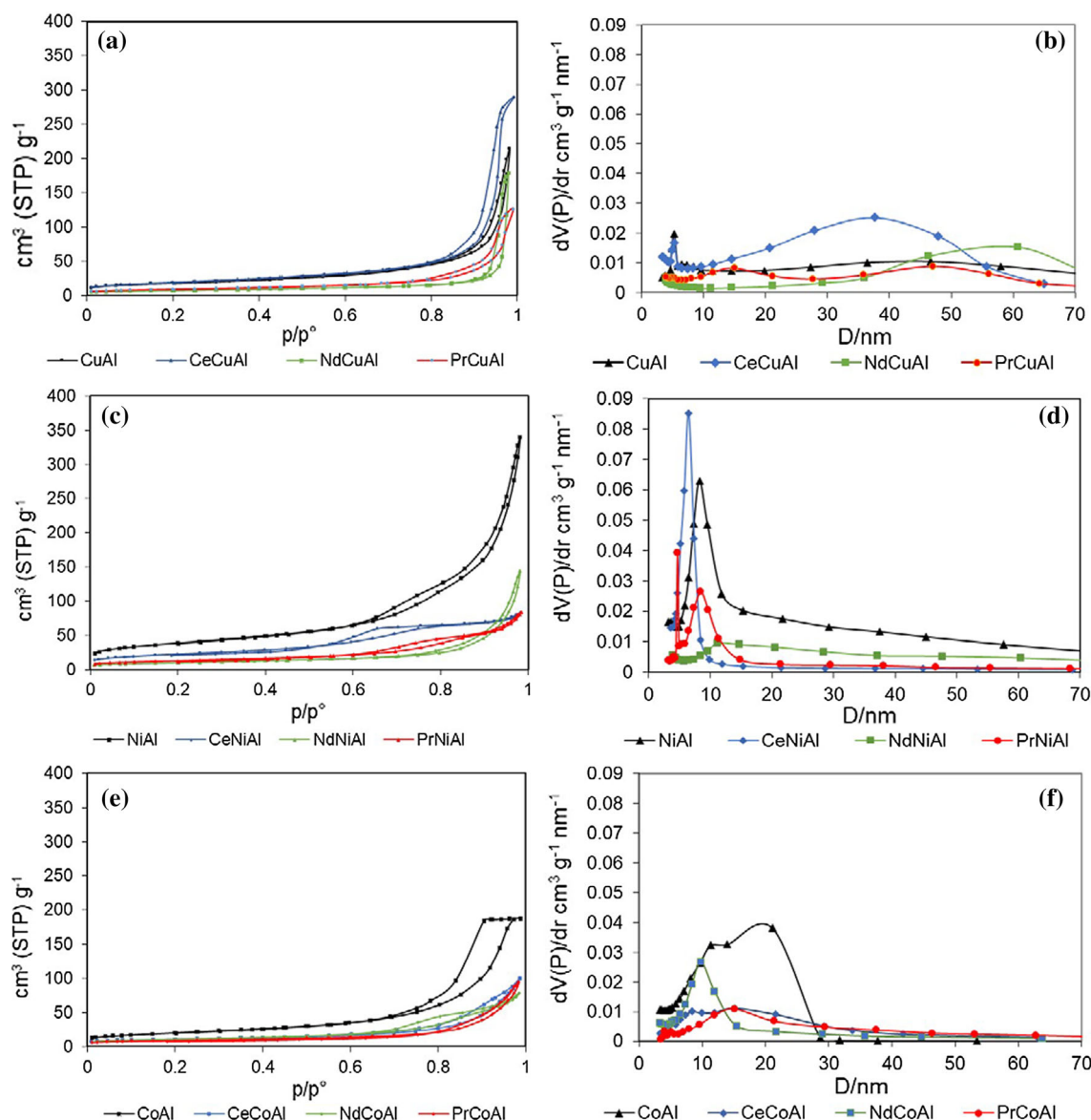
Figure 3 N₂ adsorption–desorption isotherms and mesopore distributions (from the desorption branch of the isotherms) of Cu- (A, B), Ni-nickel (C, D), and Co-containing catalysts (E, F).

The materials of the Ni- and Co-containing series presented a different distribution of porosity. Both NiAl and CoAl featured a bimodal pore size distribution, with a peak of intergranular porosity at 8 nm for NiAl and 11 nm for CoAl, followed by a different distribution of a larger secondary porosity. The addition of REE brought to the virtual disappearance of the secondary porosity, leaving only an intergranular porosity with a size related to the average size of nanocrystals. For all these materials, the pore volume was in reasonable agreement with the Gurvitch estimate, as expected from the narrower pore

size distribution. It can be expected that Cu-bearing materials, with a large pore volume between aggregates of nanoparticles, present better accessibility to the reactant molecules during deN₂O than the Ni- and Co-bearing materials, with a narrower distribution of smaller pores.

H₂-TPR of catalysts and benchmark materials

The reducibility of mixed oxide catalysts was studied by H₂-TPR in the range 50–900 °C. The hydrogen consumptions of all catalysts are summarized in

Table 2 Hydrogen consumption in H_2-TPR, light-off temperature and apparent activation energy of N_2O conversion

Sample code	H_2 consumption / mmol g^{-1}	T_{50} / °C	E_a / kJ mol^{-1}
CuAl	9.97	445	115
CeCuAl	5.71	390	71
NdCuAl	4.98	385[a]	56
PrCuAl	5.74	415	102
NiAl	9.29	425	95
CeNiAl	5.76	425	81
NdNiAl	5.98	325	43
PrNiAl	5.20	345	63
CoAl	12.79	395	45
CeCoAl	6.84	300/420[a]	10
NdCoAl	6.41	315/435[a]	19
PrCoAl	7.06	330	13

[a] In harsh conditions (1000 ppm N_2O + 200 ppm NO + 20,000 ppm O_2 + 2500 ppm H_2O/N_2)

Table 2 together with data on their catalytic activity in N_2O decomposition (light-off temperature, 50% N_2O converted, T_{50}). Before considering the effect of REE, it is interesting to compare the reduction patterns of the samples CuAl, NiAl, and CoAl, prepared by calcination of HT, with the H_2-TPR traces of the corresponding single cation oxides prepared by the same alkali precipitation method, as shown in Fig. 4.

CuAl, NiAl, and CoAl showed some increase in the temperature of reduction by comparison with the corresponding pure transition metal oxides (Fig. 4). The hydrogen consumption of both CuAl and CuO started around 130 °C but the reduction of copper oxide to metallic copper was completed at 350 °C on CuO and 400 °C on CuAl, despite the lower amount of CuO present in the latter sample (Fig. 4A) [47]. This effect is similar to the delayed reduction of CuO when deposited in a limited amount on γ-Al_2O_3 support, the lower reducibility being attributed to strong oxide-support interaction [48]. The absence of a defined copper aluminate phase is confirmed by the absence of the reduction peak of $CuAl_2O_4$ around 500 °C [49].

The hydrogen consumption of NiAl started at 370 °C and the reduction to metallic Ni was completed at 850 °C, whereas the reduction of pure NiO started at 270 °C and was completed at 550 °C (Fig. 4B). The much lower reducibility of NiO formed by thermal decomposition of LDHs has been
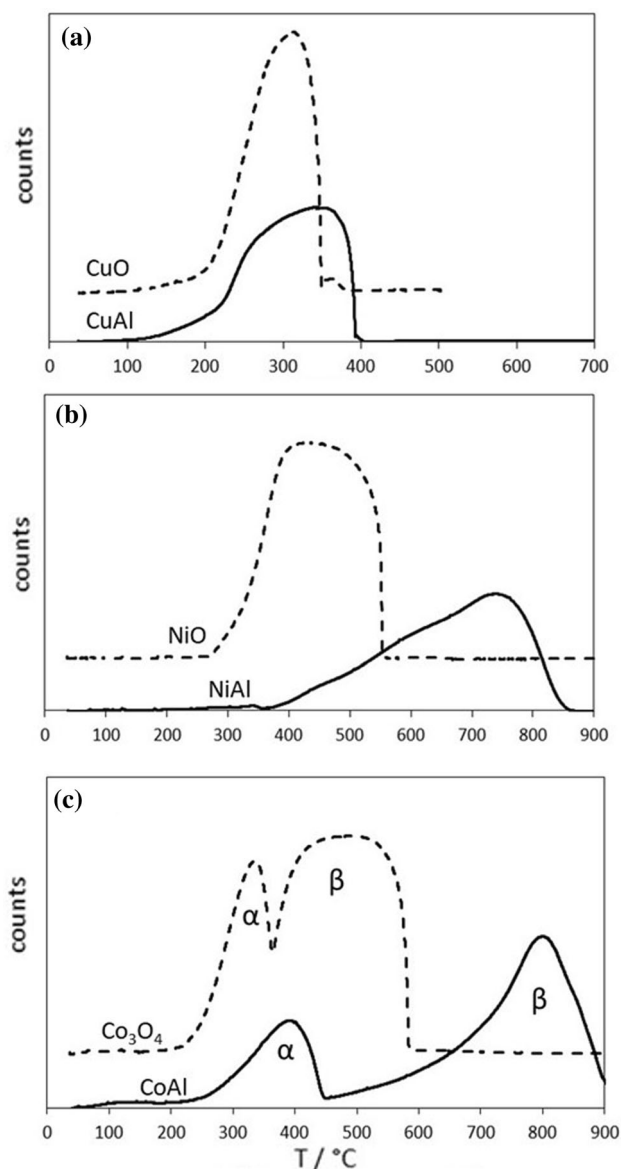
Figure 4 H_2-TPR traces of MO_x oxides with M = (A) Cu, (B) Ni, (C) Co and their corresponding MAl oxides.

attributed to the formation of a Ni–Al oxide solid solution at the surface of the NiO crystals exsoluted in the early steps of calcination [39, 50]. The presence of such a surface solid solution accounts for the lower reducibility and the negative skewness of the reduction peak, its final temperature being compatible with the expected reduction temperature of bulk nickel aluminate phases in the range of 825–875 °C [51].

The hydrogen consumption on Co_3O_4 starts at 220 °C and presents two peaks, α at 345 and β at 486 °C, and is completed at 590 °C (Fig. 4C). The ratio of H_2 consumed between the β and α peak is 2.8,

in good agreement with the ratio 3 expected for the attribution of α peak to the reduction of spinel to CoO and of the β peak to the reduction of the divalent oxide to metal. Also, the sample CoAl presents two peaks, the β peak having an H_2 consumption exactly three times the one of α peak. However, both peaks are skewed to a much higher temperature than in pure Co_3O_4. Albeit the ratio 3 between the H_2 consumptions of β and α peaks disproves high incorporation of Al in the spinel, it is clear that the interaction with Al-bearing materials dramatically decreases the reducibility of cobalt spinel. The reduction of Co_3O_4 begins at 230 °C, is completed at 450 °C and is immediately followed by a negatively skewed β peak of reduction of CoO, the reduction being virtually completed at 900 °C. This shift to high temperatures is observed also in the reduction of cobalt oxide catalysts supported on γ-Al_2O_3 by several preparation methods [52]. However, complete reduction of CoAl is obtained at a somewhat higher temperature than in other instances [45, 53].

The effect of the addition of REE on the reducibility of the materials can be observed on both the shape of H_2-TPR traces and H_2 consumption (Table 2, Fig. 5 and Fig. S1).

For the CuAl series, Ce addition introduced early reduction phenomena starting at 95 °C, whereas Nd and Pr did not significantly alter the initial reduction temperature (Fig. 5A). The low-temperature H_2 consumption of CeCuAl likely corresponds to the reduction of well-dispersed CuO species in interaction with CeO_2 [54]. It has been observed that a strong interaction between CuO and CeO_2 can result in a weakened Cu–O bond, easily reducible at lower temperatures [19, 21]. For all rare earth-bearing samples—NdCuAl, PrCuAl and CeCuAl, the reduction of CuO was completed at lower temperatures than for CuAl, due to the lower amount of copper species in samples containing around 55% mass of rare earth oxides.

For the NiAl series, the addition of REE did not modify the onset temperature of the main H_2 consumption peak at 370 °C but introduced small reduction phenomena at a lower temperature (Fig. 5B). This indicates the presence of species in which the Ni–O bond was weakened by a "separation effect" due to the presence of high contents of rare earth oxides in interaction with nanocrystallites of NiO, analogous to the effect of high content of La_2O_3 in the Ni/Al_2O_3 catalyst [36]. Indeed, the small peaks
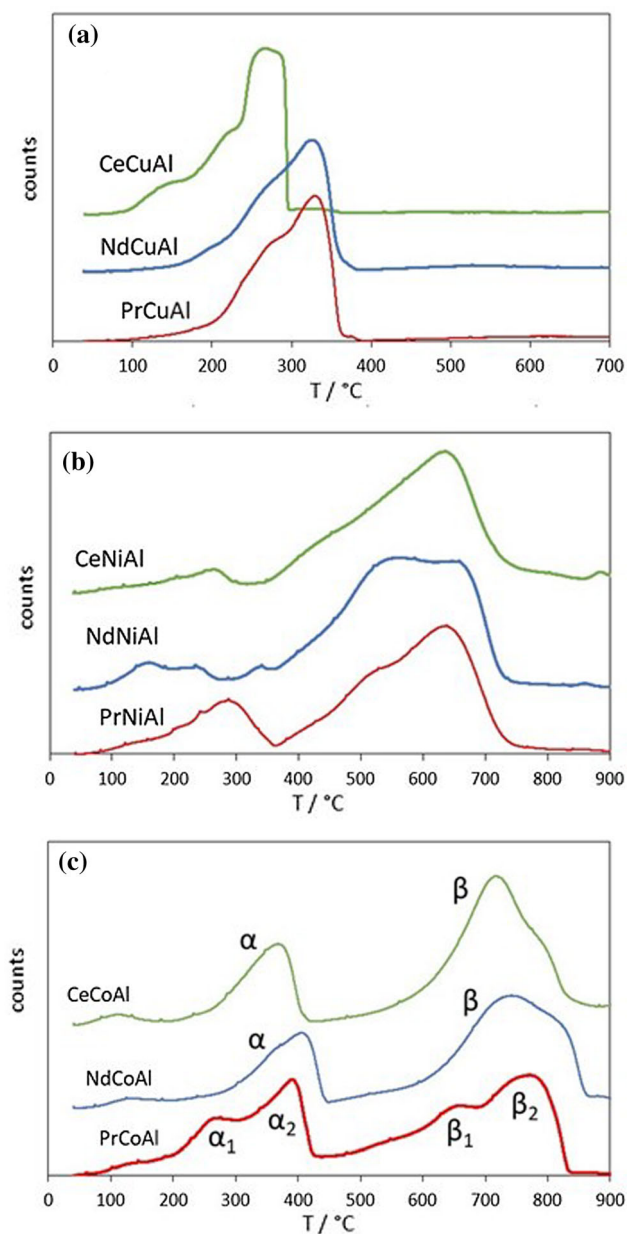
Figure 5 H_2-TPR traces of different RMAl mixed metal oxides with R = Ce, Nd, Pr and M = Cu (A), Ni (B), Co(C).

at lower temperatures (160, 270, and 290 °C for NdNiAl, CeNiAl, and PrNiAl, respectively) were reasonably close to those reported for low loading of Ni interacting with LnO_x (Ln = Ce, Pr) [20, 55]. These low-temperature reduction phenomena were by no means negligible, as they represented 8, 10 and 21% of the total H_2 consumption for CeNiAl, NdNiAl, and PrNiAl, respectively. Literature data suggest that a minor contribution of the reduction of PrO_x could also not be discarded [53]. As in the case of the Cu-bearing samples, the final temperature of reduction

of the rare-earth-bearing samples was lower than that for NiAl, largely due to the lower amount of NiO in the samples.

In the case of the Co-bearing sample, the onset temperature of the reduction of the cobalt spinel was not affected by the presence of REE in CeCoAl and NdCoAl, which presented minor low-temperature reduction phenomena at about 120 °C (Fig. 5C). In the case of PrCoAl, instead, the H_2 consumption began at 90 °C and evolved with no solution of continuity toward a two-pronged α peak, with maxima, α_1 at 270 and α_2 at 390 °C. Also, the β peak was split, with two maxima, β_1 at 660 and β_2 at 770 °C. This indicated the presence of two types of spinel particles, differing by their reactivity. The ratio of H_2 consumption between β and α peaks is 1.5, i.e., much lower than the ratio 3 expected for a two-step reduction of Co_3O_4 to metal through a CoO intermediate. A component of direct reduction of Co_3O_4 to metal in the α peak has been reported in some literature instances [50]. In the case of PrCoAl, it is clear (Fig. 5C) that the α peak is superposed to the onset of the extremely skewed β peak, supporting the assumption that reduction of a significant fraction of spinel to Co metal has taken place at low temperatures.

Catalytic activity in deN₂O

Figure 6 shows the comparison of the catalytic activity and the apparent activation energy of the pristine MAl and REE-modified catalysts, whereas Table 2 presents the value of temperature at which 50% of N_2O is converted. A blank test without catalyst showed a conversion of N_2O below 1% in the temperature range of 50–600 °C under 1000 ppm N_2O/N_2, suggesting that the contribution of non-catalytic activity was negligible during the catalytic tests. The comparison of the light-off temperature (50% N_2O converted, T_{50}) of the pristine materials revealed an increase of activity in the increasing order of CuAl ($T_{50} = 445$ °C) < NiAl ($T_{50} = 425$ °C) < CoAl ($T_{50} = 385$ °C) (Fig. 6 A, B, C). Full N_2O conversion was reached at 500 °C for both CoAl and NiAl, but only at 550 °C for CuAl catalyst. A similar trend was reported by Kannan for hydrotalcite-derived mixed metal oxides with a M/Al ratio 3 [7].

All REE-containing materials exhibited considerably higher activity than the pristine catalysts. An exception was CeNiAl, which showed almost the same activity as pristine NiAl. However, the enhancement in the catalytic activity of the modified catalysts does not follow the same trend for CuAl, CoAl, and NiAl series, suggesting that the activity of materials depends both on the pristine system and the nature of the introduced REE. For CuAl series, the order of activity in term of T_{50} increased as follows: CuAl ($T_{50} = 445$ °C) < PrCuAl ($T_{50} = 415$ °C) < CeCuAl ($T_{50} = 390$ °C) ∼ NdCuAl ($T_{50} = 385$ °C). In the NiAl series, the order was NiAl ($T_{50} = 425$ °C) = CeNiAl ($T_{50} = 425$ °C) < < PrNiAl ($T_{50} = 345$ °C) < NdNiAl ($T_{50} = 325$ °C) and, for the CoAl series, it was CoAl ($T_{50} = 395$ °C) < < PrCoAl ($T_{50} = 330$ °C) < NdCoAl ($T_{50} = 315$ °C) < CeCoAl ($T_{50} = 300$ °C). The order in the apparent activation energies followed the same trend as the light-off temperature (Table 2). It should be noted that the catalytic activity did not strongly correlate with the materials' textural properties. For example, the specific surface areas of the REE-containing materials were lower than those of the pristine catalysts (except the case of CeCuAl), and this trend did not follow the order of the catalytic activity. Thus, the catalytic activity of N_2O decomposition was probably related to the enhancement of the redox properties rather than the textural properties of the materials with the addition of REE.

In the case of the NiAl-derived catalysts, the introduction of REE in NdNiAl and PrNiAl decreased the T_{50} by 100 and 80 °C, respectively, while no change of catalytic activity was observed with the introduction of Ce in CeNiAl. This trend is related to the reduction onset temperature of the samples in H_2-TPR. NdNiAl and PrNiAl present significant reduction phenomena at 120–150 °C, not observed in the case of CeNiAl. Interestingly, no mixed crystalline phases were observed in any of these samples, suggesting that the enhancement of reduction and catalytic properties is not related to the presence of a specific crystalline phase.

The CuAl-related catalysts were the less active of our samples, both in the presence or the absence of REE. The introduction of REE induced a decrease of T_{50} lower than in all Cu-free catalysts, with the already observed exception of CeNiAl. The CeCuAl catalyst has a much lower reduction temperature than NdCuAl (Fig. 5A), whereas it has an activity being close to the latter. This could be explained by the nature of the REE oxides since CeO_2 is well-known for the presence of oxygen vacancy, and it
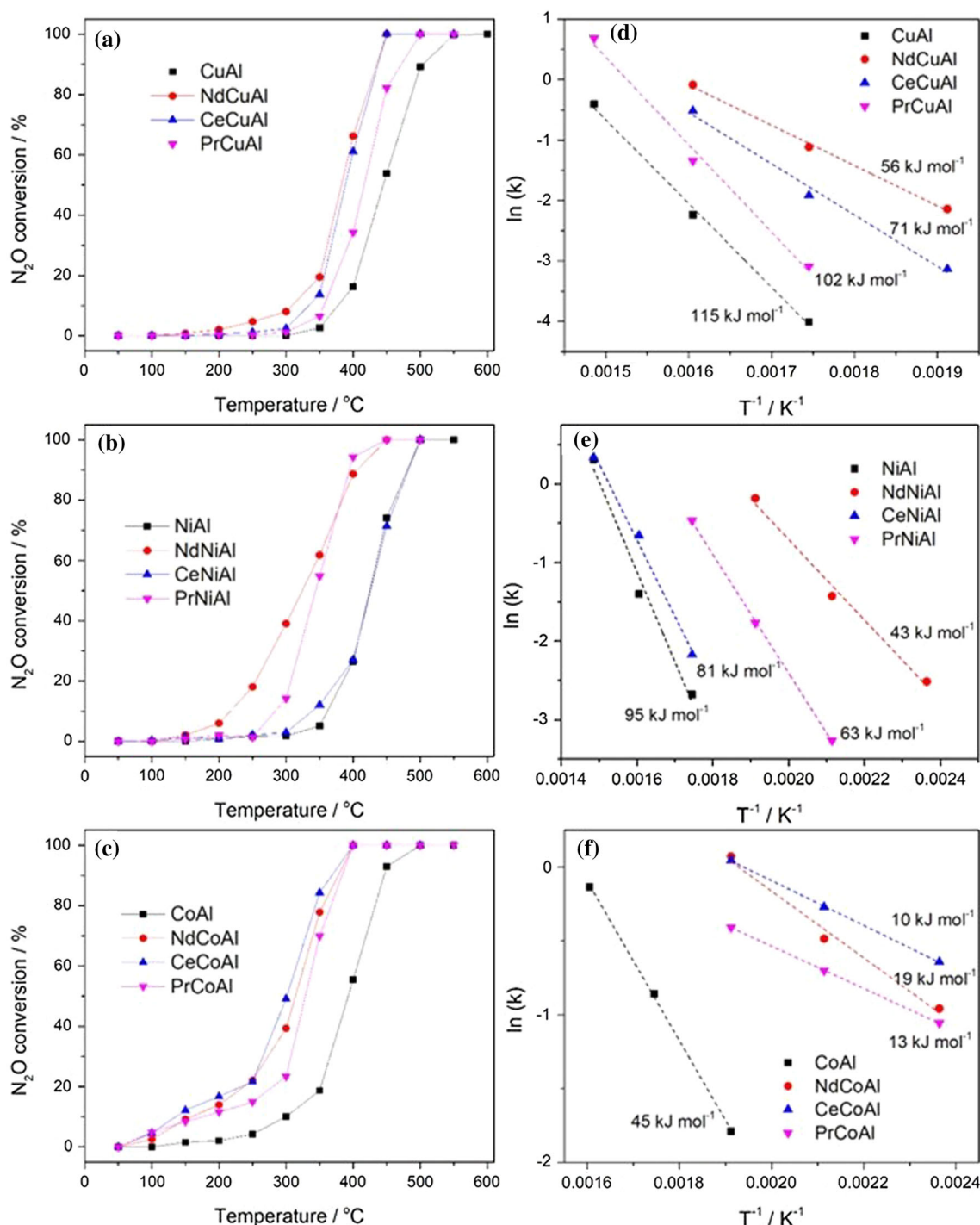
Figure 6 N_2O conversion (A, B, C) and Arrhenius plots for calculation of apparent activation energy(D, E, F) of different RMAl mixed metal oxides (R = Nd, Ce, Pr and M = Cu, Ni, Co). Reaction conditions: 0.3 g catalyst, 80 mL min^{-1} of 1000 ppm N_2O/N_2. To minimize the influence of heat generated from the exothermic reaction, E_a calculations were performed for data points with conversion lower than 30%.

also has a higher surface area than Nd_2O_3, which could influence the particle size of CuO and hence the reduction temperature. Secondly, CuO was dispersed on the CeO_2 and Al_2O_3 mixed oxides in CeCuAl (i.e.,

Cu^+/Cu^{2+} redox pair) [5], whereas in NdCuAl, copper species appeared as the new phase of Nd_2CuO_4 (i.e., Cu^{2+}/Cu^{3+} redox pair) [56]. The presence of the Nd_2CuO_4 phase explained the effect of Nd

loading on the activity of the CuNdAl system reported in our previous study [32].

The CoAl-related catalysts were the most active of our samples, with and without the addition of REE. The order of enhancement of activity (CeCoAl > NdCoAl > PrCoAl > > CoAl) corresponds to the improvement of the reducibility of the samples with the insertion of REE (see Table 2 and Fig. 5). All REE introduced low-temperature reduction phenomena, which were extremely relevant in the case of the initial reduction peak at 120 °C observed for CeCoAl and NdCoAl.

The effectiveness of oxide catalysts for N_2O decomposition has been attributed to the simultaneous presence of oxygen vacancies, favoring N_2O adsorption, and redox sites, able to split the N–O bond [57]. In the presence of cations with variable oxidation states, the two effects can be related, the reduction of the surface cations easily inducing oxygen vacancies. In our results, no clear correlation occurred between the presence of mixed crystalline phases and the initial steps of reduction of the materials. Likely, in the case of the insertion of REE in transition metal oxides on alumina, the most relevant effect for catalysis was the formation of a limited amount of easily reducible MO_x sites, related to surface compositional defects. In the case of HT-derived oxides, the presence of LnO_x seems to have affected reducibility by a mechanism related to the competition of the large REE cations with the HT phase in the precipitation of the precursors. The formation of oxides by calcination of compositionally disordered materials, with a less defined interaction of MO_x with Al, has likely favored the formation of coordinative defects, more liable to induce oxygen vacancies and the mixed-valence states conducive to easier catalyst regeneration [5, 58]. It is also worth remembering that the introduction of REE in NiAl and CoAl materials led to a significant decrease in the size of NiO and Co_3O_4 nanocrystals (see Table S1), with an increase of the extent of the interface between MO_x and other components. Such an effect was not observed in the case of the CuO crystals in CuAl materials, for which the introduction of REE led to a much lower enhancement of reduction and catalytic properties.

The CeCoAl catalyst was very promising, with T_{50} at 300 °C and full conversion at 400 °C. It was accordingly further tested under harsher conditions of 1000 ppm N_2O, 200 ppm NO, 20 000 ppm O_2, and 2500 ppm H_2O/N_2. T_{50} shifted to around 420 °C

(approximately 120 °C higher than that for tests carried out in 1000 ppm N_2O/N_2 (Fig. 7A). Stability tests were performed in these conditions at 450 °C for 50 h as well as in ideal conditions (1000 ppm N_2O/N_2) for 30 h (Fig. 7B). In the ideal condition, at 350 °C the catalyst showed around 76% conversion of N_2O. The conversion slightly increased to 81% after 20 h time-on-stream (TOS) and stayed stable for the last 10 h of the test. A similar trend was observed in a harsher condition test at 450 °C. In the beginning, the catalyst exhibited 87% N_2O conversion. After 22 h TOS, the conversion increased gradually to 90% and stayed constant for the remaining 28 h of the total 50 h TOS (Fig. 7B). This level of conversion in the
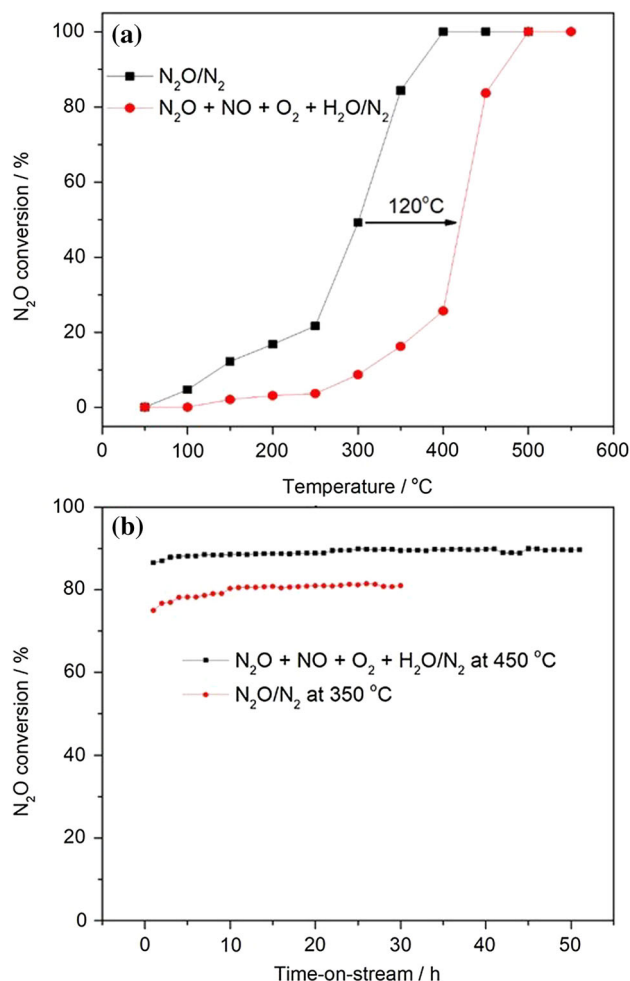
Figure 7 Catalytic activity of CeCoAl catalyst: (A) Comparison of absence and presence of inhibitors and (B) Stability test in absence and presence of inhibitors. Reaction conditions: 0.3 g catalyst, 80 mL min^{-1} of 1000 ppm N_2O/N_2 (absence of inhibitors) or 1000 ppm N_2O + 200 ppm NO + 20000 ppm O_2 + 2500 ppm H_2O/N_2 (presence of inhibitors).
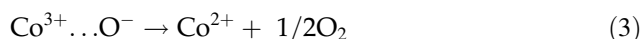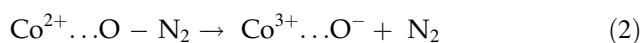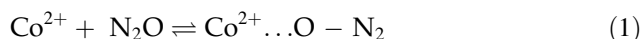
Table 3 Comparison of the catalytic activity in deN$_2$O with Cu-, Ni-, and Co-based catalysts given in the recent literature

Mixed metal oxides	Preparation method (Calcination temperature / °C)	Reaction conditions	N$_2$O conversion / % (temperature / °C)	Ref
Co-CeO$_2$ K/Co-CeO$_2$ (5 mol.% Ce)	Coprecipitation (400)	500 ppm N$_2$O/N$_2$, or *wet conditions 500 ppm N$_2$O, 30 000 ppm O$_2$, 30 000 ppm H$_2$O/ N$_2$, GHSV 45,000 h^{-1}	50 (340) 50 (320*)	61
CoMnAl (4/1/1 mol.% ratio)	Coprecipitation (500)	1000 ppm N$_2$O/He, 0.1 g catalyst, SV = 60 L g^{-1} h^{-1}	50 (∼ 410)	62
1.4% Na/CoMnAl 1.8% K/CoMnAl	Coprecipitation + impregnation (500)		50 (∼ 380) 50 (∼ 335)	
MnCoAl FeCoAl (0.175/3/1 mol.% ratio)	Coprecipitation (600)	1000 ppm N$_2$O/N$_2$, or * harsh conditions 1000 ppm N$_2$O, 45 000 ppm O$_2$, 300 ppm NO /N$_2$, 0.35 g catalyst, 100 mL min^{-1} (WHSV = 17 L g^{-1} h^{-1})	50 (305) 50 (376*) 50 (327) 50 (380*)	63
Cu$_{0.25}$Co$_{2.75}$O$_4$ K/Cu$_{0.25}$Co$_{2.75}$O$_4$ (mol.% ratio)	Thermal decomposition (600)	1000 ppm N$_2$O/N$_2$, or * wet conditions 1000 ppm N$_2$O, 20 000 ppm O$_2$, 200 ppm NO, 5000 ppm H$_2$O/N$_2$, W/F = 0.2 g s mL^{-1} (WHSV = 18 L g^{-1} h^{-1})	50 (∼ 340) 50 (∼ 500*) 50 (∼ 260) 50 (∼ 420*)	64
(1.0wt.%)AgCoAl (0.7wt.%)AgCoAl (3/1 mol.% ratio)	Coprecipitation (600)	1000 ppm N$_2$O/N$_2$, or * harsh conditions 1000 ppm N$_2$O, 45 000 ppm O$_2$, 300 ppm NO /N$_2$, 0.35 g catalyst, 100 mL min^{-1} (WHSV = 17 L g^{-1} h^{-1})	50 (265) 89 (400*) 50 (305) 50 (390*)	65
NdCuAl NdCoAl (0.5/0.8/0.2, mol. ratio)	Coprecipitation (600)	1000 ppm N$_2$O/N$_2$, or * wet conditions 1000 ppm N$_2$O, 20 000 ppm O$_2$, 200 ppm NO, 2500 ppm H$_2$O/N$_2$, 0.30 g catalyst, 80 mL min^{-1}	50 (385) 50 (315, 435*) 60 (450*, 50 h)	32
CeCoAl (0.5/0.8/0.2, mol. ratio)	Coprecipitation (600)	1000 ppm N$_2$O/N$_2$, or * wet conditions 1000 ppm N$_2$O, 20 000 ppm O$_2$, 200 ppm NO, 2500 ppm H$_2$O/N$_2$, 0.30 g catalyst, 80 mL min^{-1}, SV = 16 L g^{-1} h^{-1}	50 (300, 420*) 86.5–89.5 (450*, 50 h)	This work

stability test is considerably higher than the 60% value reported for the NdCoAl catalyst under the same harsh conditions [32]. The mechanism of the N$_2$O decomposition on CeCoAl catalyst could be proposed via a three-step reaction [24, 59, 60] in which the redox properties of Co^{2+}/Co^{3+} pairs respond for the dissociation of N$_2$O molecules (Eq. 1) and the formation of oxygen adsorbed species (Eq. 2). The addition of CeO$_2$, i.e., the Ce^{3+}/Ce^{4+} pairs, is responsible for the diffusion and recombination of

the adsorbed oxygen species which enhance the desorption of the adsorbed O$^-$ and subsequently the regeneration of the active sites (Eq. 3).

$$Co^{2+} + N_2O \rightleftharpoons Co^{2+}\ldots O-N_2 \qquad (1)$$

$$Co^{2+}\ldots O-N_2 \rightarrow Co^{3+}\ldots O^- + N_2 \qquad (2)$$

$$Co^{3+}\ldots O^- \rightarrow Co^{2+} + 1/2 O_2 \qquad (3)$$

In summary, the reactivity of the catalysts modified by REE increased despite the addition of nearly 55%

w/w REE brought to a significant decrease in the amount of Cu, Ni, and Co in the samples. The improvement of the catalytic activity with the introduction of REE was related to the enhanced low-temperature reducibility of the catalyst and could be tuned by the choice of the REE-MAl couple.

A brief comparison of the catalytic activity of the CeCoAl catalyst with Co-based catalysts from recent literature is presented in Table 3. For instance, either CoCeO$_x$ (5% mol. Ce) or Co$_4$Mn$_1$Al$_1$ promoted by alkaline metals showed slightly lower activity than the CeCoAl catalyst of this work [61, 62]. The catalytic activity of CeCoAl was similar to Mn-(Fe) promoted Co$_3$Al$_1$-O$_x$ hydrotalcite-derived materials [63]. CeCoAl outperformed Cu$_{0.25}$Co$_{2.75}$O$_4$ (T$_{50}$ ∼ 340 and 500 °C in similar conditions on dry and wet feedstock) and was comparable with the one promoted by K, K/Cu$_{0.25}$Co$_{2.75}$O$_4$ (T$_{50}$ ∼ 420 °C in similar conditions on wet feedstock) [64]. Remarkably, the reactivity of the CeCoAl catalyst was quite close to the noble metal-bearing (0.7 wt.%) Ag-Co$_3$Al-O$_x$ catalyst [65]. This suggests that the CeCoAl material is a promising noble metal-free catalyst for the decomposition of N$_2$O.

Conclusions

Mixed metal oxides R$_{0.5}$M$_{0.8}$Al$_{0.2}$ (R = Ce, Nd, Pr; M = Cu, Ni, Co) were prepared via coprecipitation followed by thermal treatment at 600 °C. In the absence of rare earth cations, the decomposition of precipitated HT phases led to the formation of MO$_x$ phases with reducibility decreased by the presence of amorphous alumina. The introduction of Ce led to the formation of discrete CeO$_2$, while Nd and Pr brought about the formation of both of their discrete oxides and mixed phases in strong interaction with transition metal cations. The formation of Ruddlesden–Popper phases was favored in the presence of Cu, while perovskite was formed in the Nd–Co system. The high loading of REE-bearing phases caused a decrease in specific surface area, except in the case of Ce$_{0.5}$Cu$_{0.8}$Al$_{0.2}$, in which the specific surface area was slightly increased by the presence of nanocrystalline CeO$_2$. Those phases co-existed with the oxide structures that originated from virgin M-AlO$_x$. Independently of the formation of new phases, the presence of REE modified the redox properties of the catalysts, either by weakening the M–O bond in

M-AlO$_x$ phases or by isolating a fraction of MO$_x$ from the interaction with Al by competition with the HT phase in the precipitation. The formation of low-temperature reducible MO$_x$ species brought to their enhanced activity in deN$_2$O. i.e., a decrease of the light-off temperature and the apparent activation energy. The most active catalyst investigated in this study, Ce$_{0.5}$Co$_{0.8}$Al$_{0.2}$, showed very stable conversion of N$_2$O without degradation for 50 h TOS under a gas feed containing inhibitors (1000 ppm N$_2$O, 200 ppm NO, 20000 ppm O$_2$, and 2500 ppm H$_2$O/N$_2$).

References

[1] Li Y, Armor JN (1992) Catalytic decomposition of nitrous oxide on metal exchanged zeolites. Appl Catal B Environ 1:L21–L29

[2] Jabłońska M, Palkovits R (2016) Nitrogen oxide removal over hydrotalcite-derived mixed metal oxides. Catal Sci Technol 6:49–72

[3] Jabłońska M, Palkovits R (2016) It is no laughing matter: nitrous oxide formation in diesel engines and advances in its abatement over rhodium-based catalysts. Catal Sci Technol 6:7671–7687

[4] Kapteijn F, Rodriguez-Mirasol J, Moulijn JA (1996) Heterogeneous catalytic decomposition of nitrous oxide. Appl Catal B Environ 9:25–64

[5] Konsolakis M (2015) Recent advances on nitrous oxide (N_2O) decomposition over non-noble-metal oxide catalysts: catalytic performance, mechanistic considerations, and surface chemistry aspects. ACS Catal 5:6397–6421

[6] Liu Z, He F, Ma L, Peng S (2016) Recent advances in catalytic decomposition of N_2O on noble metal and metal oxide catalysts. Catal Surv Asia 20:121–132

[7] Kannan S (1998) Decomposition of nitrous oxide over the catalysts derived from hydrotalcite-like compounds. Appl Clay Sci 13:347–362

[8] Imamura S, Tadani JI, Saito Y, Okamoto Y, Jindai H, Kaito C (2000) Decomposition of N_2O on Rh-loaded Pr/Ce composite oxides. Appl Catal A Gen 201:121–127

[9] Rico-Pérez V, Parres-Esclapez S, Illán-Gómez MJ, Salinas-Martínez de Lecea C, Bueno-López A (2011) Preparation, characterisation and N_2O decomposition activity of honeycomb monolith-supported $Rh/Ce_{0.9}Pr_{0.1}O_2$ catalysts. Appl Catal B Environ 107:18–25

[10] Parres-Esclapez S, Illán-Gómez MJ, M.d. Lecea CS, Bueno-López A, (2012) Preparation and characterisation of γ-Al2O3 particles-supported $Rh/Ce_{0.9}Pr_{0.1}O_2$ liucatalyst for N_2O decomposition in the presence of O_2, H_2O and NO_x. Int J Greenh Gas Con 11:251–261

[11] Christopher J, Swamy CS (1991) Studies on the catalytic decomposition of N_2O on $LnSrFeO_4$ (Ln=La, Pr, Nd, Sm and Gd). J Mol Catal 68:199–213

[12] Dacquin JP, Lancelot C, Dujardin C, Da Costa P, Djega-Mariadassou G, Beaunier P, Kaliaguine S, Vaudreuil S, Royer S, Granger P (2009) Influence of preparation methods of $LaCoO_3$ on the catalytic performances in the decomposition of N_2O. Appl Catal B Environ 91:596–604

[13] Kumar S, Vinu A, Subrt J, Bakardjieva S, Rayalu S, Teraoka Y, Labhsetwar N (2012) Catalytic N_2O decomposition on $Pr_{0.8}Ba_{0.2}MnO_3$ type perovskite catalyst for industrial emission control. Catal Today 198:125–132

[14] Pan KL, Yu SJ, Yan SY, Chang MB (2014) Direct N_2O decomposition over La_2NiO_4-based perovskite-type oxides. J Air Waste Manage 64:1260–1269

[15] Jabłońska M, Palkovits R (2019) Perovskite-based catalysts for the control of nitrogen oxide emissions from diesel engines. Catal Sci Technol 9:2057–2077

[16] Perez-Alonso F, Melian-Cabrera I, Lopez-Granados M, Kapteijn F, Fierro J (2006) Synergy of $Fe_xCe_{1−x}O_2$ mixed oxides for N_2O decomposition. J Catal 239:340–346

[17] Iwanek E, Krawczyk K, Petryk J, Sobczak JW, Kaszkur Z (2011) Direct nitrous oxide decomposition with CoO_x-CeO_2 catalysts. Appl Catal B Environ 106:416–422

[18] Adamski A, Zając W, Zasada F, Sojka Z (2012) Copper ionic pairs as possible active sites in N_2O decomposition on CuO_x/CeO_2 catalysts. Catal Today 191:129–133

[19] Zhou H, Huang Z, Sun C, Qin F, Xiong D, Shen W, Xu H (2012) Catalytic decomposition of N_2O over $Cu_xCe_{1−x}O_y$ mixed oxides. Appl Catal B Environ 125:492–498

[20] Zhou H, Hu P, Huang Z, Qin F, Shen W, Xu H (2013) Preparation of NiCe mixed oxides for catalytic decomposition of N_2O. Ind Eng Chem Res 52:4504–4509

[21] Zabilskiy M, Erjavec B, Djinović P, Pintar A (2014) Ordered mesoporous CuO–CeO_2 mixed oxides as an effective catalyst for N_2O decomposition. Chem Eng J 254:153–162

[22] Zabilskiy M, Djinović P, Erjavec B, Dražić G, Pintar A (2015) Small CuO clusters on CeO_2 nanospheres as active species for catalytic N_2O decomposition. Appl Catal B Environ 163:113–122

[23] Zabilskiy M, Djinović P, Tchernychova E, Tkachenko OP, Kustov LM, Pintar A (2015) Nanoshaped CuO/CeO_2 materials: effect of the exposed ceria surfaces on catalytic activity in N_2O decomposition reaction. ACS Catal 5:5357–5365

[24] Grzybek G, Stelmachowski P, Gudyka S, Indyka P, Sojka Z, Guillén-Hurtado N, Rico-Pérez V, Bueno-López A, Kotarba A (2016) Strong dispersion effect of cobalt spinel active phase spread over ceria for catalytic N_2O decomposition: the role of the interface periphery. Appl Catal B Environ 180:622–629

[25] Zabilskiy M, Djinović P, Tchernychova E, Pintar A (2016) N_2O decomposition over CuO/CeO_2 catalyst: new insights into reaction mechanism and inhibiting action of H_2O and NO by operando techniques. Appl Catal B Environ 197:146–158

[26] Liu Z, He C, Chen B, Liu H (2017) CuO-CeO_2 mixed oxide catalyst for the catalytic decomposition of N_2O in the presence of oxygen. Catal Today 297:78–83

[27] You Y, Chang H, Ma L, Guo L, Qin X, Li J, Li J (2018) Enhancement of N_2O decomposition performance by N_2O pretreatment over Ce-Co-O catalyst. Chem Eng J 347:184–192

[28] Xue L, He H, Liu C, Zhang C, Zhang B (2009) Promotion effects and mechanism of alkali metals and alkaline earth metals on cobalt−cerium composite oxide catalysts for N_2O decomposition. Environ Sci Technol 43:890–895

[29] Xue L, Zhang C, He H, Teraoka Y (2007) Promotion effect of residual K on the decomposition of N_2O over cobalt–cerium mixed oxide catalyst. Catal Today 126:449–455

[30] Xue Z, Shen Y, Shen S, Li C, Zhu S (2015) Promotional effects of Ce^{4+}, La^{3+} and Nd^{3+} incorporations on catalytic performance of Cu–Fe–O_x for decomposition of N_2O. J Ind Eng Chem 30:98–105

[31] Abu-Zied BM, Bawaked SM, Kosa SA, Ali TT, Schwieger W, Aqlan FM (2017) Effects of Nd-, Pr-, Tb- and Y-doping on the structural, textural, electrical and N_2O decomposition activity of mesoporous NiO nanoparticles. Appl Surf Sci 419:399–408

[32] Ho PH, Jablonska M, Nocuń M, Fornasari G, Ospitali F, Vaccari A, Palkovits R, Benito P (2019) Effect of neodymium in Co(Cu)-Al mixed oxides on their physico-chemical properties and activity in N_2O decomposition. ChemCatChem 11:5580–5592

[33] (1997) The Lanthanide Elements (Z = 58–71). In: Greenwood NN, Earnshaw A (eds.) Chemistry of the Elements (2nd Edition). Butterworth-Heinemann, Oxford, pp 1227–1249.

[34] Bîrjega R, Pavel OD, Costentin G, Che M, Angelescu E (2005) Rare-earth elements modified hydrotalcites and corresponding mesoporous mixed oxides as basic solid catalysts. Appl Catal A Gen 288:185–193

[35] Rodrigues E, Pereira P, Martins T, Vargas F, Scheller T, Correa J, Del Nero J, Moreira SGC, Ertel-Ingrisch W, De Campos CP, Gigler A (2012) Novel rare earth (Ce and La) hydrotalcite like material: synthesis and characterization. Mater Lett 78:195–198

[36] Zhang L, Lin J, Chen Y (1992) Characterization of dispersion and surface states of NiO/γ-alumina and NiO/La_2O_3–γ-alumina catalysts. J Chem Soc, Faraday Transactions 88:497–502

[37] Toby BH (2001) EXPGUI, a graphical user interface for GSAS. J Appl Cryst 34(2):210–213

[38] Larson AC, Von Dreele RB (1994) General Structure Analysis System (GSAS), Los Alamos National Laboratory, Report LAUR 86–748. https://11bm.xray.aps.anl.gov/documents/GSASManual.pdf. Accessed 08 February 2021

[39] Neimark AV, Ravikovitch PI (2001) Capillary condensation in MMS and pore structure characterization. Micropor Mesopor Mat 44:697–707

[40] Trifirò F, Vaccari A, Clause O (1994) Nature and properties of nickel-containing mixed oxides obtained from hydrotalcite-type anionic clays. Catal Today 21:185–195

[41] Rives V, Kannan S (2000) Layered double hydroxides with the hydrotalcite-type structure containing Cu^{2+}, Ni^{2+} and Al^{3+}. J Mater Chem 10:489–495

[42] Hill RJ, Craig JR, Gibbs GV (1979) Systematics of the Spinel Structure Type. Phys Chem Minerals 4:317–339

[43] Imai H, Tagawa T, Wada S (1990) Formation of cubic Ln_2O_3 crystallites in amorphous $LnAlO_3$ mixed oxide particles (Ln = rare-earth metal). J Mater Sci Lett 9:56–57. https://doi.org/10.1007/BF00724432

[44] Muschick W, Müller-Buschbaum H (1977) About the crystal chemistry of three-valent rare earth oxides the stabilisation of the monoclinic B-modification. Z Naturforsch 33:495–498

[45] Lowell S, Shields JE, Thomas MA, Thommes M (2004) Characterization of Porous Solids and Powders: Surface Area. Pore Size and Density, Springer, Neitherlands

[46] Rouquerol J, Rouquerol F, Llewellyn P, Maurin G, Sing K (2013) Adsorption by Powders and Porous Solids, 2nd edn. Academic Press

[47] Jabłońska M, Arán MA, Beale AM, Góra-Marek K, Delahay G, Petitto C, Pacultová K, Palkovits R (2019) Catalytic decomposition of N_2O over Cu–Al–Ox mixed metal oxides. RSC Adv 9:3979–3986

[48] Yu QC, Zhang SC, Yang B (2011) Dispersion of copper oxide supported on γ-alumina and its sulfation properties. Trans Nonferrous Met Soc China 21:2644–2648

[49] Luo MF, Fang P, He M, Xie YL (2005) In situ XRD, Raman, and TPR studies of CuO/Al_2O_3 catalysts for CO oxidation. J Mol Catal A Chem 239:243–248

[50] Tichit D, Medina F, Coq B, Dutartre R (1997) Activation under oxidizing and reducing atmospheres of Ni-containing layered double hydroxides. Appl Catal A Gen 159:241–258

[51] Salhi N, Petit C, Kiennemann A (2008) Steam reforming of methane on nickel aluminate defined structures with high Al/Ni ratio. In: Gédéon A, Massiani P, Babonneau F (eds) Zeolites and Related Materials: Trends. Elsevier, Targets and Challenges, pp 1335–1338

[52] Jacobs G, Ji Y, Davis BH, Cronauer DC, Kropf AJ, Marshall CL (2007) Fischer-Tropsch synthesis: Temperature programmed EXAFS/XANES investigation of the influence of support type, cobalt loading, and noble metal promoter addition to the reduction behaviour of cobalt oxide particles. Appl Catal A Gen 333:177–191

[53] Obalová L, Pacultová K, Balabánová J, Jirátová K, Bastl Z, Valášková M, Lacný Z, Kovanda F (2007) Effect of Mn/Al ratio in Co–Mn–Al mixed oxide catalysts prepared from hydrotalcite-like precursors on catalytic decomposition of N_2O. Catal Today 119:233–238

[54] Jabłońska M, Nothdurft K, Nocuń M, Girman V, Palkovits R (2017) Redox-performance correlations in Ag–Cu–Mg–Al,

Ce–Cu–Mg–Al, and Ga–Cu–Mg–Al hydrotalcite derived mixed metal oxides. Appl Catal B Environ 207:385–396

[55] Alcalde-Santiago V, Davó-Quiñonero A, Lozano-Castelló D, Quindimil A, De-La-Torre U, Pereda-Ayo B, González-Marcos JA, González-Velasco JR, Bueno-López A (2018) Ni/LnO$_x$ Catalysts (Ln=La, Ce or Pr) for CO$_2$ Methanation. ChemCatChem 11:810–819

[56] Hiroyuki Y, Taihei N, Noritaka M, Makoto M (1993) Catalytic decomposition of nitrogen monoxide over valency-controlled la$_2$cuo$_4$-based mixed oxides. Bull Chem Soc Jpn 66:3492–3502

[57] Xiong S, Chen J, Huang N, Yang S, Peng Y, Li J (2019) Balance between reducibility and N$_2$O adsorption capacity for the N$_2$O decomposition: Cu$_x$Co$_y$ catalysts as an example. Environ Sci Technol 53:10379–10386

[58] Russo N, Fino D, Saracco G, Specchia V (2007) N$_2$O catalytic decomposition over various spinel-type oxides. Catal Today 119:228–232

[59] Chellam U, Xu ZP, Zeng HC (2000) Low-Temperature Synthesis of Mg$_x$Co$_{1-x}$Co$_2$O$_4$ Spinel Catalysts for N$_2$O Decomposition. Chem Mater 12:650–558

[60] Asano K, Ohnishi C, Iwamoto S, Shioya Y, Inoue M (2008) Potassium-doped Co$_3$O$_4$ catalyst for direct decomposition of N$_2$O. Appl Catal B Environ 78:242–249

[61] Kim MJ, Lee SJ, Ryu IS, Jeon MW, Moon SH, Roh HS, Jeon SG (2017) Catalytic decomposition of N$_2$O over cobalt based spinel oxides: the role of additives. Mol Catal 442:202–207

[62] Karásková K, Obalová L, Kovanda F (2011) N$_2$O catalytic decomposition and temperature programmed desorption tests on alkali metals promoted Co–Mn–Al mixed oxide. Catal Today 176:208–211

[63] Jabłońska M, Arán MA, Beale AM, Delahay G, Petitto C, Nocuń M, Palkovits R (2019) Understanding the origins of N$_2$O decomposition activity in Mn(Fe)CoAlO$_x$ hydrotalcite derived mixed metal oxides. Appl Catal B Environ 243:66–75

[64] Franken T, Palkovits R (2015) Investigation of potassium doped mixed spinels CuxCo$_{3-x}$O$_4$ as catalysts for an efficient N$_2$O decomposition in real reaction conditions. Appl Catal B Environ 176–177:298–305

[65] Jabłońska EM, Buselli L, Nocuń EM, Palkovits R (2018) Silver-doped cobalt (magnesium) aluminum mixed metal oxides as potential catalysts for nitrous oxide decomposition. ChemCatChem 10:296–304